Computational Intelligence Methods for Underwater Magnetic-based Protection Systems

Sergio Decherchi, Davide Leoncini, Paolo Gastaldo, Rodolfo Zunino, Osvaldo Faggioni, and Maurizio Soldani

***Abstract*— Magnetic-based detection technologies for undersea protection systems are very effective in monitoring critical areas where weak signal sources are difficult to identify (e.g. diver intrusion in proximity of the seafloor). The complexity of the involved geomagnetic phenomena and the nature of the target detection strategy require the use of adaptive methods for signal processing. The paper shows that Computational Intelligence (CI) models can be integrated with those magnetic-based technologies, and presents an effective, reliable system for adaptive undersea protection. Two different CI paradigms are successfully tested for the specific application task: Circular BackPropagation (CBP) and Support Vector Machines (SVMs). Experimental results on real data prove the advantage of the integrated approach over existing conventional methods. Individual CI components and the overall detection system have been verified in real experiments.**

I. Introduction

TARGET detection and intrusion prevention are crucial issues in undersea and port protection systems. The complexity of the involved problems and the lack of established models of the underlying phenomena have raised an increasing interest for adaptive paradigms such as Machine Learning and Neural Networks [1-4].

In the specific scope of intrusion detection, neural classifier tools have already been successfully coupled with sonar-based systems [1-4] to enhance accuracy in target detection [5]. Sonar technology is very effective in the monitoring of obstruction-free large volumes of water, but may fail in the presence of acoustically shadowed spots. This typically occurs in the proximity of the seafloor and is due to echo, reverberation, and others issues related to the morphology of the sea bottom [6]. Magnetic-based detection systems have proved effectively in those critical conditions where peripheral sensing is required [7]. Indeed, the current trend in the design of high-accuracy, high-reliability protection systems is to couple sonar-based and magnetic-sensing technologies, and to endow them with complementary missions [7].

In fact, the topology configuration and the operational deployment of a magnetic-based detection system is a critical issue due to: 1) the intrinsic, highly non-linear magnetic noise from the environment (e.g. a port, human activity, anomalies in solar activity), and 2) the peculiar nature of the weak signal sources associate with the targets of interest (e.g., divers). Moreover, an intrusion detection system should be also robust against random malfunctioning of the sensing devices. Thus magnetic-sensing technologies need to be enhanced by the nonlinear representation and the classification ability of machine-learning models for accurate detection.

The novelty aspects of the presented research mainly lie in the integration of machine learning tools in a magnetic-based sensing architecture and in a design strategy to select the adequate paradigm in such a context. This methodology results in a highly accurate, highly reliable and robust detection system aimed at diver intrusion prevention and port protection. The approach involves two supervised classifier models for target detection and identification: Support Vector Machines [8] and Circular Back Propagation Networks [9].

II. Architectures for Magnetic-Based Detection Systems

A. Geomagnetic Phenomena for Weak Signal Detection

The adoption of the geomagnetic field for target detection allows one to manage critical scenarios that are not covered by other technologies (e.g., weak signal detection, protection of acoustically blind areas, etc). At the same time, one has to tackle a complex phenomenon, which results from the superposition of several magnetic fields generated by natural and artificial sources. Sources can be both internal and external to Earth, and are characterized by different physical qualities (i.e. form, position, etc…).

The classical detection approach highlights the magnetic characteristics of the target by separating them from the overall (geo)magnetic field. It requires an accurate modeling of the geomagnetic field, and assumes that one can single out and classify every magnetic source that generates interesting signals. In practice, an analyst typically tunes a bank of devices by adjusting the characteristic frequencies of Low-Pass, Band-Pass, and High- Pass Filters. The actual filter settings depend on: 1) the magnetic sources of information that are associated with the targets, and 2) the signals that are therefore predicted by the model. This method exhibits some crucial drawbacks and nowadays is regarded as ineffective,

S. Decherchi, D. Leoncini, P. Gastaldo and R. Zunino are with the DIBE - Dept. Biophysical and Electronic Eng., University of Genoa, Genova, ITALY (e-mail: {sergio.decherchi, davide.leoncini, paolo.gastaldo, rodolfo.zunino}@unige.it).

O. Faggioni and M. Soldani are with the National Institute of Geophysics and Volcanology, Portovenere, ITALY (e-mail: {osvaldo.faggioni, maurizio.soldani}@ingv.it).

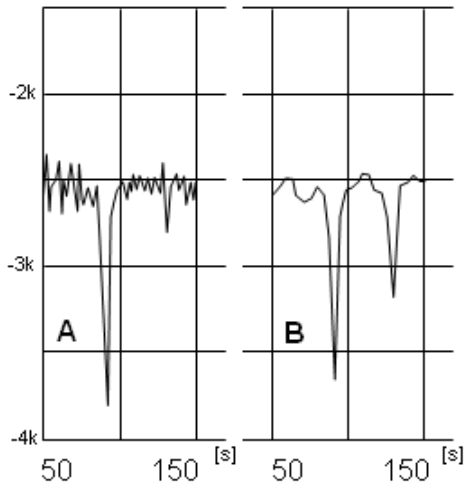

Fig. 1. Comparison between the adaptive (A) and the classical (B) detection approach on a real diver-intrusion test. The classical filtering approach (involving the total magnetic field only) induces a false-positive.

especially for the detection of weak signals [7]. This is mainly due to the complexity of the observed phenomenon which prevents the refinement of an accurate model of the measured field.

An alternative approach extracts the magnetic signal of the target by means of a flexible noise-cancellation technique, which does not make any assumption about the observed environment [7]. The critical operation of this method is an adaptive filtering procedure, in which one measures the background (noise) signal, and uses the empirical results to cancel the noise term from the total observed field; this ultimately highlights the information of interest. Such an approach does not imply any subjective setting of filters, but requires a careful sensing of the environmental noise.

The simplest adaptive set-up involves a twin-sensor configuration, in which one device captures the overall signal (also including target contributions), whereas the other measures the "reference" environmental magnetic noise. The proper displacement of the sensing devices clearly becomes a critical aspect to ensure a correct acquisition of the target-independent noise component [7]. Previous research [10] developed and tested the design guidelines for the proper topological configuration of the devices. When, ideally, both sensors are perfectly synchronized, a simple subtraction between the two measures highlights the target signal.

Figure 1 compares the classical and the adaptive detection techniques in the time domain [s], under the above assumption of synchronization. Side A shows the differential field measured by the adaptive system [10], in which the reference signal is subtracted to the target signal; the peak marks a diver intrusion that is correctly detected. Side B gives the result obtained by the classical approach, which applies LPF to the overall signal (environment and target); the graph shows that environmental noise induced a false positive (the secondary peak).

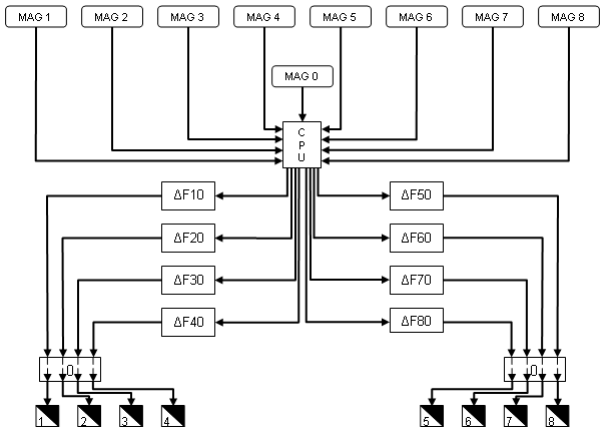

Fig. 2. RIMAN adaptive configuration: the array of magnetometers are referred to one reference sensor (MAG0). Each blocks Δ*Fn*0 supports the adaptive target detection of the *n*-th sensor.

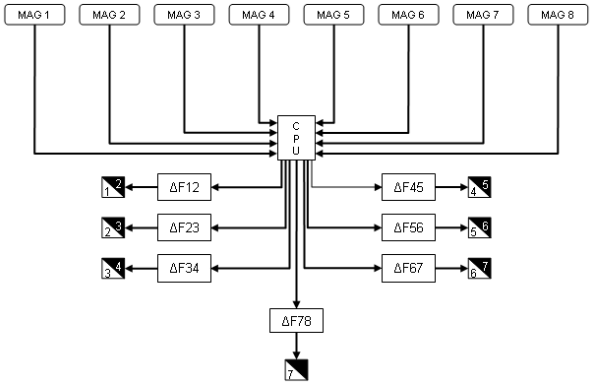

Fig. 3. SIMAN configuration: each magnetometer operates both as a sentinel and as a reference for neighboring devices. Block Δ*Fmn* supports the adaptive target detection for the pair of sensors MAG*m* and MAG*n*.

B. Architectures for adaptive magnetic-based detection

The adaptive approach leads to two possible supporting architectures. In the basic schema, an array of "sentinel" magnetometers are all coupled with one separate device, which provides the "reference" measures of the noise signal to be canceled. This architecture is called RIMAN-type (Referred Integrated MAgnetic Network) configuration [10], and is shown in Fig.2

The Self-referred Integrated MAgnetic Network (SIMAN) schema improves on the basic RIMAN system; it includes an array of sensors in which, at the same time, every instrument operates as a sentinel and as the reference for the neighboring magnetometers [10]. Figure 3 shows the overall SIMAN architecture.

The approach presented in this paper implements a SIMAN configuration and includes, for the sake of simplicity and without loss of generality, a pair of magnetometers. In practice, at least three devices should be deployed in order to break symmetry and allow the detection of half-way crossing targets; nevertheless the twin-device experimental configuration is suitable for the validation of the system under a wide range of operational conditions.

C. Critical issues in the detection strategy

The integration of a reference and a sentinel signal greatly enhances detection effectiveness because it makes it possible to bypass the requirement of an accurate model of the observed environment. At the same time, the differential nature of the overall principle dictates strict design guidelines and poses some relevant issues.

First of all, the assumption of sensor synchronization is mostly unrealistic in real scenarios, which involve several magnetometers with non-ideal physical characteristics; misalignments in the time domain affect the detection system in the form of signal random perturbations. The latter terms add up to the inherent noise component that results from the imperfect coherence between the sentinel and the reference sources, due to the spatial displacement of the sensors.

Another critical aspect in the tuning of the pairwise architecture stems from the spurious signals that may be prompted by individual magnetometers during the sensing procedure. Spurious phenomena are only due to a defective behavior of the device; they appear in the form of extremely brief spikes and can mislead the detection system if they are not properly recognized as false alarms. These anomalous impulse signals affect most current magnetometers and are quite difficult to predict, since they are not related to the measurement procedure but only depend on the physical characteristic of the sensors.

The above variety of external critical issues exhibits a complex operational problem, whose main aspects are the highly nonlinear nature of the involved phenomena and the practical difficulty to predict the behavior of system components. The general crucial issue actually is the absence of any model of the overall scenario.

These considerations justify the adoption of empirical methods to support the detection system. The detection principle itself calls indeed for adaptive paradigms, which can adjust their performance in compliance with environmental conditions and specific signals. From this viewpoint, the field of computational Machine Learning (ML) techniques offers a wide spectrum of suitable methodologies, and the present research shows that ML-related paradigms can cover virtually the entire range of requirements for an effective deployment of the adaptive magnetic-based detection technologies.

III. Computational Intelligence Methods for Magnetic-Based Detection

The main issues that are raised by magnetic-based detection technologies can be summarized in the following requirements: first, specific and reliable paradigms should support the critical parts of the process, such as target detection and event classification; second, one needs some quantitative method to validate the obtained results and compare the alternative solutions objectively. Computational intelligence techniques aim at building predictive systems that can make reliable decisions on unseen samples. As a result, these paradigms can fit the magnetic-detection requirement quite effectively.

This paper focuses on two alternative techniques: Support Vector Machines (SVM) [8] and Circular BackPropagation (CBP) [9], which extends the classical MultiLayer Perceptron (MLP).

A. Classification Algorithms for Magnetic-Based Detection

The training of learning systems requires a dataset, X, holding n patterns (samples): each pattern includes a data vector, $\mathbf{x} \in R^m$, and the category label, $y \in \{-1, +1\}$. When developing data-driven classifiers, the learning phase requires both $\mathbf{x}$ and y to build up a decision rule. After training, the system can process data that do not belong to the training set; the system classifies each input sample with a predicted category, $\hat{y} \in \{-1, +1\}$.

The function that predicts the class of a sample is the decision function, $\hat{y} = \text{sign}(f(\mathbf{x}))$, where $f(\mathbf{x})$ is a weighted sum of non linear basis functions. The resulting trained system, thus, can be easily implemented in an electronic device for real-time data processing, thanks to the straightforward expression of decision function.

In the case of SVM, generalization ability relies on two main concepts: the function $f(\mathbf{x})$ belongs to a Reproducing Kernel Hilbert Space (RKHS), and Regularization Theory is used as the conceptual basis [8]. The decision function $f_{\text{SVM}}(\mathbf{x})$ can be written as:

$$f_{SVM}(\mathbf{x}) = \sum_{i}^{n_{sv}} \alpha_i y_i K(\mathbf{x}_i, \mathbf{x}) + b \qquad (1)$$

where, $K(,)$ is a kernel function [8] and the number of Support Vectors n_{sv} , the 'bias' term b and coefficients α_i are computed by the training algorithm [8], which minimizes a quadratic cost function [8]. The eventual generalization performance of a SVM depends on the specific setting of the scalar parameter C that regulates the trade-off between accuracy and complexity in the training process [8], and the kernel-specific parameters. In this work, the classical RBF kernel has been adopted.

CBP is a single-layer feedforward network that connects the input layer to the hidden layer (having N_h neurons) through a set of weights. The CBP network, in particular, augments the conventional MultiLayer Perceptron (MLP) architecture with an additional input, being the sum of the squared values of all the network inputs. As a result, the overall decision function, $f_{\text{CBP}}(\text{x})$ is given by:

$$f_{CBP}(\mathbf{x}) = \sum_{j=1}^{N_h} w'_j a_j(\mathbf{x}) + b' \qquad (2)$$

where

$$a_j(\mathbf{x}) = sigm\left(\sum_{i=1}^{m} w_{ji} x_i + w_{j,m+1} \sum_{i=1}^{m} x_i^2 + b \right) \qquad (3)$$

Coefficients $\mathbf{w}$, $\mathbf{w}'$ are denoted as "weights," b and b′ are a bias. Theory proves that feed-forward networks embedding a sigmoidal activation function, $\text{sigm}(r) = (1+e^{-r})-1$, can

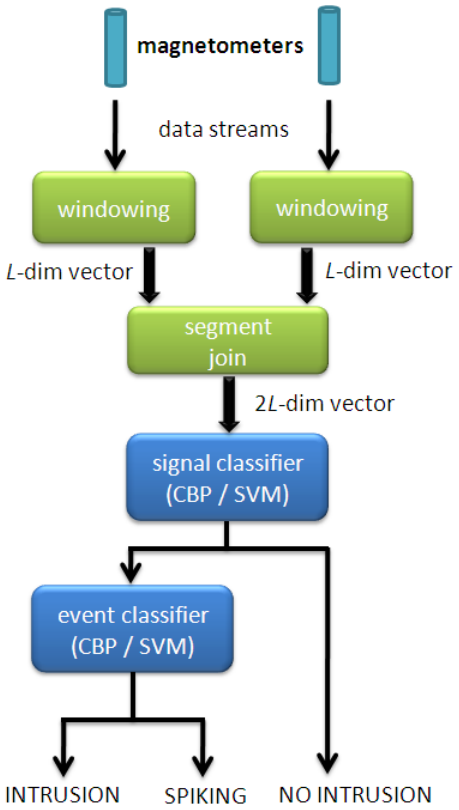

Fig. 4. The processing architecture of the overall neural magnetic-based detection system.

support arbitrary mappings [11]. The quadratic term in (3) allows the CBP network either to adopt the standard sigmoidal behavior, or a bell-shaped radial function, depending on the data. As a major result, the CBP network does not need any a-priori assumption to formulate the model without affecting the fruitful properties of an MLP structure. The structural CBP enhancement still allows adopting conventional back-propagation algorithms [9] for weight adjustment, yielding an effective training.

IV. The Adaptive Detection System

A. The Overall Architecture

This Section presents the architecture that integrates Computational Intelligence paradigms within the magnetic-based detection technologies, and illustrates the complete on-line processing chain that maps input signals into a decision result at run time.

The data provided by the sensory system consist in a reference signal and in a target signal; to preserve as much as possible the original information content within data, both input streams are not either pre-filtered or processed in any way. This ensures that the result of the learning process in the adaptive neural component is not affected, hence no a-priori processing of signals might bias the inductive learning process.

Each input stream is segmented by applying a conventional windowing technique: the target and reference signal is arranged into frames including L samples; the resulting windows are allowed to overlap. The amount of overlap determines a tradeoff between sample size and information consistency: indeed, a small overlap reduces the number of patterns in a sample and mitigates the mutual correlation between time-consecutive input patterns; at the same time, too small an overlap extension might affect information consistency among loosely correlated patterns.

The research presented in this paper aims at an objective evaluation of the overall method effectiveness, hence the preservation of the informative power of input signals is important. Thus the largest overlap (window size = $L - 1$) between time-consecutive frames is adopted, and for an original stream having length h, the total number of patterns (windows) is $n_p = h - L + 1$.

As a result, the input space to the neural network components joins the stream segments from the reference and the sentinel sensors, and is therefore represented by a vector having dimensionality $m = 2L$. Since this strategy generates a huge amount of patterns, a random sub-sampling technique can reduce the final cardinality of the dataset for training the system. To facilitate the numerical convergence of the training algorithms, the generated dataset is normalized in the range [-1,+1] for each time instant: in other words arranging samples data in a n_p by m matrix, normalization in [-1,+1] is performed on each column.

The output information prompted by the neural detection systems adopts a hierarchical event-labeling schema: a preliminary classifier (Signal Classifier) module discriminates Normal Signal (NS) patterns from Anomalous Signal (AS); a subsequent targeted Event Classifier module processes the AS input streams and separates Target Signal events (TS, e.g., a diver intrusion) from Sensor Spiking signals (SS, i.e., an anomalous sensing malfunctioning in a magnetometer). Both classifier stages are supported by adaptive neural components described in the previous Section, and are trained empirically.

The architecture described in Fig. 4 presents some degrees of freedom in the choice of the neural technologies that actually support the various components. The adaptive nature of the design criteria allows one to complete that selection in compliance with the specific application context depending on empirical measures.

B. Random Projection Methods for Visualization and Domain Inspection

Applications in critical domains sometimes require some justification of the empirical models; visual inspection obtained by feature reductions techniques can support such a demand. The research presented in this paper adopts Random Projections (RP) techniques [12] for that purpose. Random Projections represent a recent, increasingly popular approach to support feature reduction in a simple and efficient way. These methods are inexpensive from a computational viewpoint and yield reliable results on

complex domains [13]; in the present context, they are used as a data-analysis tool to support visual inspection of the observed domain.

The RP formalism stems from the following fundamental result on manifolds [12]:

Johnson-Lindenstrauss lemma (JL-Lemma) [13]: *For any $0 < \varepsilon < 1$ and any integer t, let k be a positive integer such that:*

$$k \geq 4(\varepsilon^2/2 - \varepsilon^3/3)^{-1} \ln(t) \quad (4)$$

Then with probability $O(1/t^2)$ for any set X of points in R^m, there is a map f: $R^m \rightarrow R^k$ such that for all x, z $\in$ X:

$$(1-\varepsilon) \leq \frac{\| f(x) - f(z) \|^2}{\| x - z \|^2} \leq (1+\varepsilon) \quad (5)$$

The function f() is rendered by projecting the original data X into the random subspace spanned by a random matrix R. This matrix is made up of d rows, k columns, every matrix entry is distributed as N(0,1) and columns have unitary length.

The JL-Lemma ensures that, when comparing the distance values between a pair of patterns in the original space {**x**,**z**} and in the mapped space {f(**x**), f(**z**)}, the distortion in distances is less than $\varepsilon \cdot \|\mathbf{x}-\mathbf{z}\|^2$. To address the projected space, $\hat{X}$, one should just build up a random matrix, *R*, (having size $d \times k$) as per JL-Lemma. Then the projected space is obtained from the original space by:

$$\hat{X} = XR \quad (6)$$

The distance-preserving property makes RP methods quite interesting for domain inspection. The mapping function, *f*, is the operational core of the overall method; if one imposes that the target space is lower-dimensional than the original one, ($k << m$) the overall framework can be regarded as a dimensionality-reduction compression process. This technique has been successfully used in text mining domains [13] for clustering purposes. In the current research, the projection method is used for solving the problem of data rendering just by imposing k=2, so that the original data are mapped into a 2-D domain allowing visual inspection.

V. Experimental Results

A. Experimental Set Up

In the experimental set-up used for the verification of the magnetic-based detection approach, the sampling frequencies for the reference and the sentinel data streams were approximately of 50 Hz. The detection response time, depended on the sampling frequency due to the window overlapping mechanism; after transient completion, the system could prompt a detection response every 0.02s (i.e. 50 Hz sampling).

To attain a robust estimation of the generalization error the set of input patterns, after sub-sampling, windowing and joining, were shuffled and split into a training and a test set; such a procedure was repeated 10 times to make up for statistical fluctuations. The eventual generalization performance was worked out by averaging the classification errors measured in the 10 runs. The overall system accuracy was evaluated by combining the accuracy measures of the pipelined classifiers, in compliance with the hierarchical schema described in the previous Section (Fig. 4).

TABLE I
Signal Classifier: the Datasets

Signal Classifier		Training set			Test set		
		–1	+1	Total	–1	+1	Total
Window size, *L*	10	268	265	533	280	251	531
	50	268	265	533	280	250	530
	100	267	265	532	278	250	528

TABLE II
Event Classifier: the Datasets

Event Classifier		Training set			Test set		
		–1	+1	Total	–1	+1	Total
Window size, *L*	10	123	142	265	106	145	251
	50	123	142	265	106	144	250
	100	123	142	265	106	144	250

An additional goal of the tests was to assess the influence of the window size, L, on the accuracy of the classifiers. Therefore, the experiments covered a set of possible window sizes: $L \in \{10, 50, 100, 200\}$. Tables I and II give the number of patterns and the distribution of classes {–1, +1} for the signal classifier and the detection-event classifier, respectively. The Tables report the cardinalities of the data sets used for training and test.

The following Sections report on the obtained results for the data-analysis process, and give the classification performances for each neural classifiers implemented.

B. Random Projection Based Data Visualization

The random-projection analysis of raw data adopted the classical approach [12], hence the entries of each random projection matrix were normally distributed as $N(0,1)$, while columns were normalized to unitary length. The space of projections always was 2-dimensional in order to allow direct visual inspection. Figures 6 and 7 present the 2-dim projection results for the signal and the event classifier, respectively; in both cases, the analysis covered different settings of the quantity, *L*, which determined the overlap between contiguous windows of sensor data.

In all graphs, cross marks and black circles mark patterns associated with opposite classes (-1, +1). A promising projection is attained when the patterns belonging to one class appear to be easily separated from those belonging to the other.

In the case of the signal classifier (Fig. 5), the graph shows that only a limited portion of patterns tended to spread out

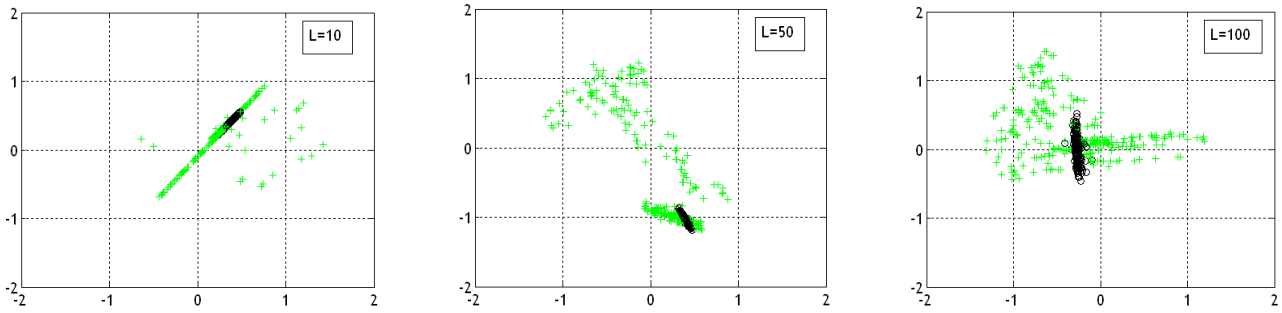

Fig.5: Signal-classifier data analysis: 2-dim Random Projections for increasing window overlap, *L*

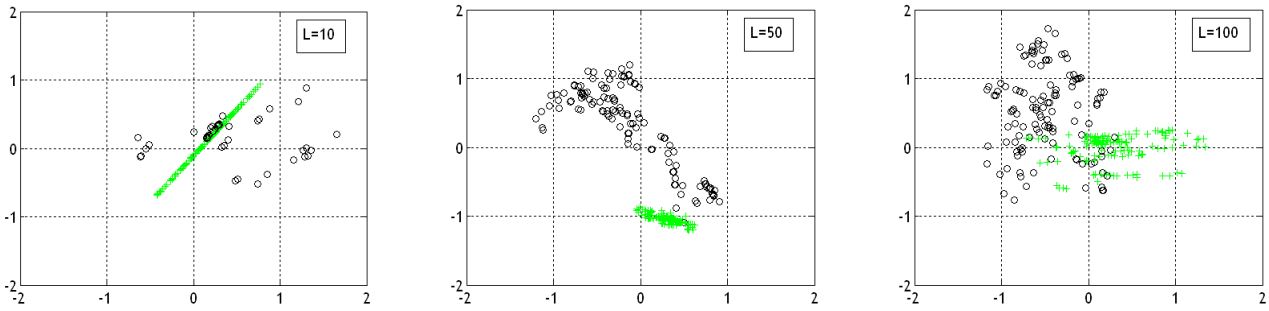

Fig.6: Event-classifier data analysis: 2-dim Random Projections for increasing window overlap, *L*

when the windows overlap extent, *L*, increased. By contrast, a marked confusion among the two classes emerged when projecting the event-classifier data (Fig. 6).

In any case, the 2-dimensional views resulting from the random-projection analysis contributed in clarifying the data distribution and the class peculiarities that could not be observed in the original, time-domain space.

C. SVM Experiments

The implementation of the Support Vector Machine model in both the Signal and the Event classifiers adopted the Radial Basis Function (RBF) kernel; such a choice was driven by a preliminary analysis [14], which had showed that other kernel formulations (such as the linear or the polynomial kernels) did not yield satisfactory accuracy levels. To tune the RBF kernel properly one should find the optimal pair of parameters $\{C, \sigma\}$ [8]. The first quantity rules the smooth shape of the learned function, the second relates to the scale of empirical data. In the case of the magnetic signals involved, the selection involved a scanning process over a ranges of values; for each pair of values, the test error on unseen data was measured. In the experiments, the tested settings were: $C, \sigma \in \{0.1, 1, 30, 60, 90, 120\}$.

The implemented SVM training procedure was based on the SMO algorithm and used the classical settings, namely, a first-order selection strategy of the working set and a tolerance setting $\tau = 1 \cdot 10^{-3}$ in the Karesh-Kuhn-Tucker optimality conditions [15]; the code was implemented as a Matlab C-coded mex-file routine.

Figures 7 and 8 give the measured classification errors on unseen test data, for the Signal and the Event classifier, respectively; the graphs also provide an estimate of the generalization performances of the various classifier settings. The *x*,*y* axes in all graphs marks the grid of tested parameter settings $\{C, \sigma\}$; the *z* axis gives the average percentage error on the test set, using different window sizes.

Figure 9 gives the overall accuracy with the optimal settings of kernel parameters $\{C, \sigma\}$ obtained from the previous analysis, and varying the window-overlap size, *L*.

The analysis of the above results pointed out that, when using the SVM model, the size of the overlap window was not a critical parameter for both the Signal and the Event Classifier. Empirical evidence also showed that the Event-Classification task seemed considerably simpler than the Signal-Classification one. This was especially true when considering the sensitivity to the kernel parameters; in the case of Event Classification, a wide range of parameters yielded good classification results, whereas such a robust behavior was not detected in the other case.

D. CBP Experiments

The set of experiments involving the Circular Back Propagation networks aimed at assessing the validity of the general detection schema, by testing an alternative model in the Signal- and the Event-classifier modules. The experiments again gave a measure of the generalization ability of the tested classifiers. The analysis was carried out

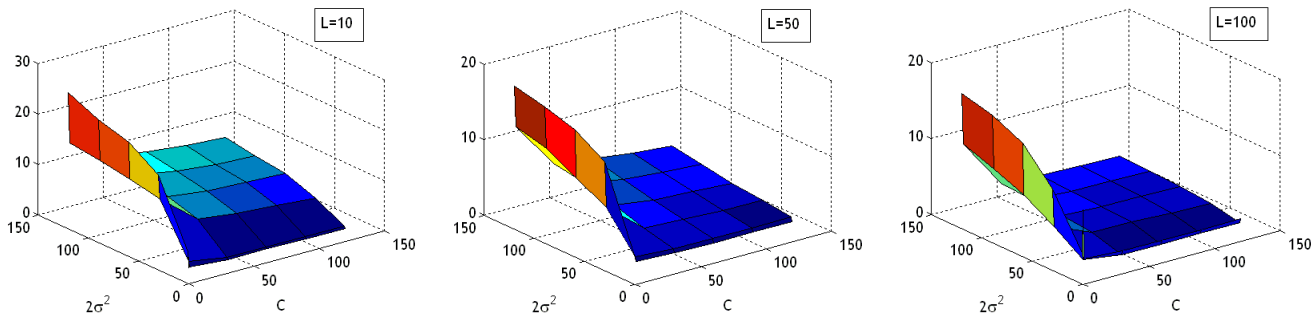

Fig.7: Signal classifier: measured test errors for different kernel parameters

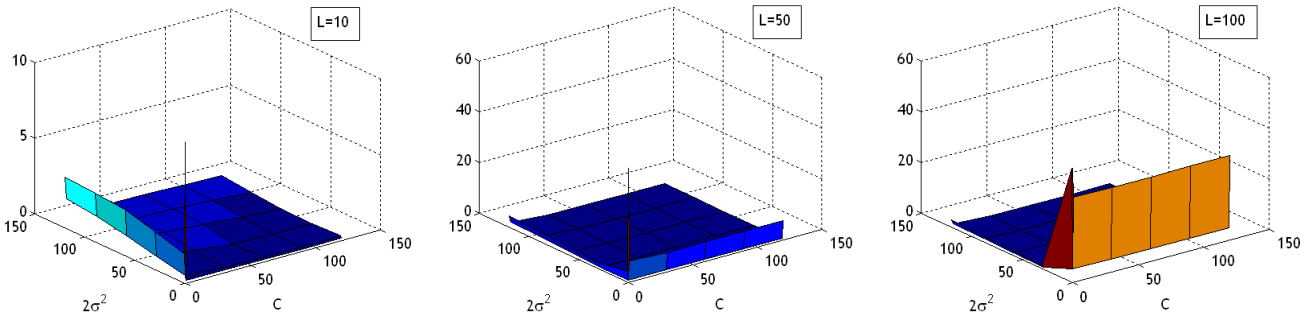

Fig.8: Event classifier: measured test errors for different kernel parameters

by testing two different topology configurations of the multilayer architecture: one configuration included 5 neurons in the hidden layer, whereas the second configuration included 10 neurons. To obtain a robust estimate of the run-time error, the training process was iterated three times and the resulting performances were averaged.

Figures 10 and 11 give the obtained results in terms of classification accuracy, while Figure 12 shows the measured detection accuracy associated with the overall detection system. An interesting element of the obtained results is that CBP-based classifiers seemed to be less sensitive to the network parameters (i.e., the number of hidden neurons) than SVM-based classifiers, and overall yielded a comparable, sometimes even better, accuracy on test data.

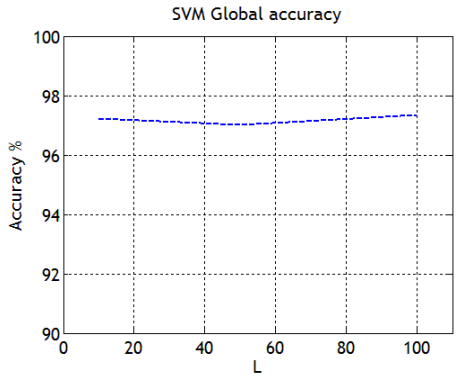

Fig. 9. Global classification accuracy for optimal kernel parameters and varying window size

VI. Conclusions

In principle, one might argue that the accuracy attained by the integrated system on the test tests did not reach the optimal level 100% and the system was subject to a few false alarms; in practice, however, this conclusion holds only when considering individual patterns. If instead one takes into account the sequential progression of empirical data, one verifies that misclassification events only occur at the transitions between normal operation and intrusion detections (or vice versa). In other words, it can be predicted theoretically, and was verified experimentally, that all misclassified patterns lied within the time intervals that spanned the beginning (or the end) of an intrusion signal. As soon as the overlap window covered a sufficient portion of the signal associated with an intrusion (or with a normal situation), the classification always proved steadily successful and complete. Such a behavior was due to the fact that, during transitions, the overlapped-window patterns involved signal samples belonging to different classes (in both the Signal and the Event classifiers), and therefore carried a degree of inherent ambiguity. The practical consequence of this phenomenon is that the system yielded a 100% accuracy, provided a delay time was allowed between the start of a change in status and the associate prompting by the system. The delay never exceeded the size, *L*, of the overlap window and on average was reasonably set to the time span covering three patterns; in a 50-Hz sampling system, this amounted to 6 ms at most.

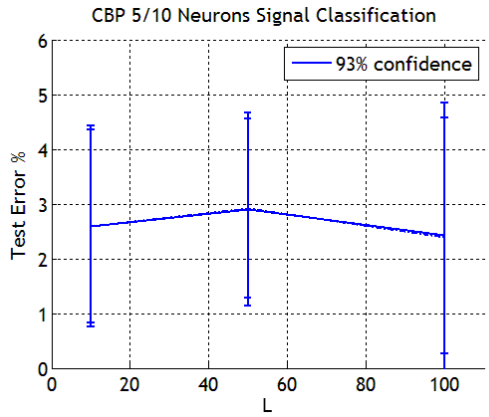

Fig. 10. Signal Classifier: CBP accuracy (5/10 hidden neurons).

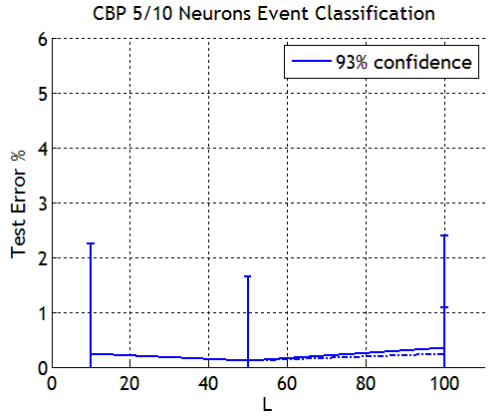

Fig. 11. Event Classifier: CBP accuracy (5/10 hidden neurons).

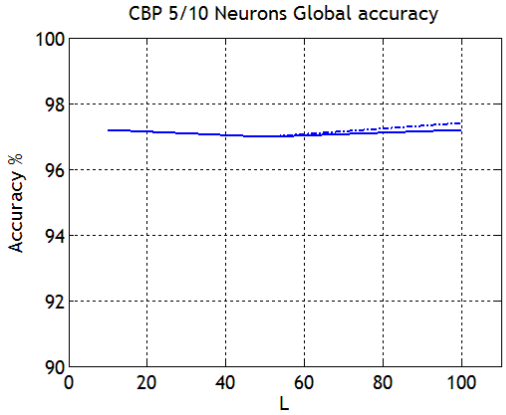

Fig. 12. Overall detection performances when using CBP networks (5/10 hidden neurons).

To perform a technical choice between the alternative classifier models for the detection system configuration, one should take into account the following aspects:

- Random Projections showed that the complexity of each classification problem involved increases when the dimensionality of the space increases;
- both the SVM and the CBP model exhibited remarkable generalization abilities.

As a consequence of those issues, one could conclude that the SVM and/or the CBP model seemed the most promising choices for further implementations on embedded platforms. The former approach, in particular, appeared in fact preferable in view of its lesser dependency on the cardinality of the input space.

ACKNOWLEDGMENT

The study of the self-informed undersea magnetic networks was launched and developed by "Ufficio Studi e Sviluppo" of COMFORDRAG – Italian Navy. This experiment was supported by Nato Undersea Research Centre.

REFERENCES

[1] D. Yao, M.R. Azimi-Sadjadi, A.A. Jamshidi, and G.J. Dobeck, "A study of effects of sonar bandwidth for underwater target classification," *IEEE Journal of Oceanic Engineering*, vol. 27, July 2002 pp. 619 - 627

[2] D. Li, M.R. Azimi-Sadjiadi, and M. Robinson, "Comparison of different classification algorithms for underwater target discrimination," *IEEE Transactions on Neural Networks*, vol. 15, Jan. 2004, pp. 189-194

[3] M.R. Azimi-Sadjadi, D. Yao, Q. Huang, and G.J. Dobeck, "Underwater target classification using wavelet packets and neural networks," *IEEE Trans. on Neural Networks*, vol. 11, May 2000, pp. 784-794

[4] M. R. Azimi-Sadjadi, D. Yao, A.A. Jamshidi, and J.G. Dobeck, "Underwater target classification in changing environments using an adaptive feature mapping," *IEEE Trans. on Neural Networks*, vol. 13, Sept. 2002, pp. 1099-1111

[5] R.P. Gorman and T.J. Sejnowski, "Analysis of Hidden Units in a Layered Network Trained to Classify Sonar Targets," *Neural Networks*, vol. 1, 1988, pp. 75-89.

[6] R.J. Urick. *Principles of Underwater Sound*. McGraw-Hill (New York), 1983.

[7] O. Faggioni, A. Gabellone, R. Hollett, R.T. Kessel, and M. Soldani, "Anti-intruder port protection MAC (Magnetic ACoustic) System: advances in the magnetic component performance," 1st WSS Conference, August 25-28, Copenhagen, Denmark, 2008.

[8] V. Vapnik, *Statistical Learning Theory*, John Wiley, New York, 1998, pp. 339-346

[9] S. Ridella, S. Rovetta, and R. Zunino, "Circular backpropagation networks for classification," *IEEE Trans. on Neural Networks*, vol. 8, no. 1, 1997, , pp. 84-97

[10] A. Gabellone, O. Faggioni, M. Soldani, and P. Guerrini, "*CAIMAN (Coastal Anti Intruder MAgnetometers Network)*," *Proc. of RTO-MP-SET-130 Symposium on NATO Military Sensing*, March 12-14, Orlando, Florida, USA, 2008, NATO classified.

[11] K. Hornik, M. Stinchcombe, and H. White, "Multilayer feedforward networks are universal approximators," *Neural Networks*, vol. 2, no. 5, pp. 359–356,1989.

[12] S. Dasgupta and A. Gupta, "An elementary proof of the Johnson–Lindenstrauss lemma", Technical report 99–006, U. C. Berkeley, March 1999.

[13] S. Decherchi, P. Gastaldo, and R. Zunino, "K-Means clustering for Content Based Document Management in Intelligence," in *Advances In Artificial Intelligence for Privacy Protection and Security*, Editors: Augusti Solanas and Antoni Martinez Bellesté, World Scientific Publishing, 2009

[14] D. Leoncini, S. Decherchi, O. Faggioni, P. Gastaldo, M. Soldani, and R. Zunino, "A Preliminary Study on SVM based Analysis of Underwater Magnetic Signals For Port Protection," *Proc. CISIS 2009*, Burgos, Spain.

[15] C.C.Chang and C.J. Lin, "LibSVM: a library for Support Vector Machines" [http://www.csie.ntu.edu.tw/~cjlin/papers/libsvm.pdf]